THE JOURNAL OF PHYSICAL CHEMISTRY C

Article

pubs.acs.org/JPCC

Stability and Electronic Properties of 2D Nanomaterials Conjugated with Pyrazinamide Chemotherapeutic: A First-Principles Cluster Study

Nabanita Saikia,* Maximilian Seel, and Ravindra Pandey*

Department of Physics, Michigan Technological University, Houghton, Michigan 49931, United States

Supporting Information

ABSTRACT: Electronic and optical properties of 2D models of graphene, boron nitride (BN), silicene, SiC, and phosphorene functionalized with pyrazinamide (PZA), a front line antitubercular chemotherapeutic, are investigated using cluster models and density functional theory with van der Waals dispersion corrections and including solvent effects. PZA favors covalent functionalization onto silicene and SiC whereas it is physisorbed onto graphene, BN, and phosphorene at a nearest-neighbor distance >3.0 Å and binding energies between −0.7 and −0.8 eV. The analysis of orbital energies, frontier orbitals, density of states, and absorption spectra shows that the HOMO−LUMO gaps for graphene, silicene, and phosphorene remain virtually unchanged upon adsorption, whereas midgap states appear in the BN and SiC clusters. For silicene, Si 2p core level photoemission spectroscopy is the better tool to analyze the chemisorption of PZA. Our study brings atomistic insight into the structural, electronic, and optical response of 2D materials as selective sensors for pyrazinamide and similar therapeutics for potential drug delivery applications.

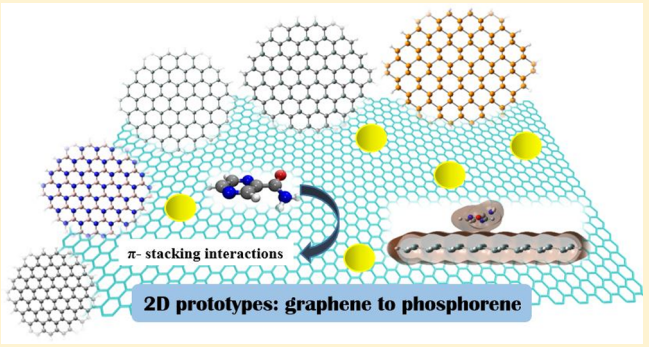

1. INTRODUCTION

The advent of engineered nanomaterials in therapeutics has seen a paradigm shift over the past few years which has opened up new avenues in health-related research areas such as multimodal drug targeting, diagnostics, and biosensing. Graphene, for that matter, has been extensively explored and exploited in the past decade owing to its inherent semimetallic characteristic coupled with other intriguing electrical and optical properties.[1−4] Given the broad spectrum of applications of graphene in nanoscale devices, 2D materials beyond graphene are currently being pursued as potential candidates for the next-generation nanoscale devices. Some of these 2D materials include boron nitride (BN), silicene, SiC, and phosphorene.

Silicene shares a honeycombed lattice similar to graphene, with high electron carrier mobility of 10^5 cm^2 V^{-1} s^{-1}.[5−7] Silicene like graphene does not have a band gap at the Fermi level,[8] and it has been reported that the spin−orbit coupling can induce a band gap within the clusters.[9] However, unlike graphene analogues, silicene has a low buckled (puckered) conformation accounted from the mixed sp^2−sp^3 hybridization, lack of π-electron delocalization, and strain induced due to mismatched hybridization.[10,11] In contrast to graphene and silicene, phosphorene is a direct band gap semiconductor with electron mobility of 1000 cm^2 V^{-1} s^{-1}, and its anisotropic electronic and optical properties originate due to the puckered honeycombed lattice.[12,13] What limits the large scale applicability of phosphorene is its facile nature to get oxidized readily on exposure to air which aids in degradation.[14] The BN cluster, isostructural to graphene, is a wide band gap 2D material due to the electronegativity variance between B and N atoms which lifts the degeneracy at the K-points in Brillouin zone.[15]

Although a wide spectra of applications of 2D materials have been foreseen and implemented, what confines the transferability to biomedical and drug targeting pursuit is the lack of detailed understanding on dispersibility of bioconjugated complexes in aqueous media (in a way to mimic the *in vivo* physiological environment). This constraint also limits the long-term biocompatibility and cytotoxicity compliance of nanomaterials. In recent years, theoretical and experimental studies have explored carbon-based nanomaterials like carbon nanotubes for drug targeting in cancer therapy and other infectious diseases.[16] The prospective opportunities of a new class of 2D nanomaterials pertaining primarily in cancer therapy have also recently been reviewed.[17]

Motivated by recent advances in synthesis and characterization of 2D nanomaterials, we now consider the feasibility of 2D materials as drug delivery agents taking PZA, as an example, because of its impact in tuberculosis (TB) therapy. It is well-known that TB is leading pathogen ranked just after cancer caused by the bacterium *Mycobacterium tuberculosis*.[18] Current therapy of TB consists of a combinatorial therapy of three

Received: June 14, 2016
Revised: August 1, 2016

DOI: 10.1021/acs.jpcc.6b06000
J. Phys. Chem. C XXXX, XXX, XXX−XXX

chemotherapeutics, namely, isoniazid (INH), pyrazinamide (PZA), and rifampin (rifampicin).[19] PZA is metabolized into its active form (pyrazoic acid) by the amidase activity of *M. tuberculosis* nicotinamidase/pyrazinamidase (MtPncA) encoded by pncA gene.[20] Nevertheless, administration of PZA in high dosage can cause detrimental health hazards, and the antibiotic resistance of bacteria under prolonged exposure triggers the need for better drug delivery systems that can target TB bacteria with enhanced selectivity, uptake, and reduced side effects. The experimental studies on host−guest complexes of cucurbit[7]uril with PZA and INH drugs showed that encapsulation helped retain drug activity via stabilization of the host−guest bioconjugates by H-bonding and hydrophobicity of the pyrazine ring.[21]

In this paper we report results of calculations regarding the response of various 2D systems toward PZA functionalization in terms of stability as well as electronic and optical properties in the aqueous medium. A cluster model approach is used; i.e., the various 2D monolayers are represented by a finite number of atoms. Specifically, we will investigate how the nature of interaction influences the electronic and optical properties of the bioconjugated complexes. Note that a noncovalent-type adsorption which induces no localized distortions within graphene, BN, and phosphorene clusters will proffer varied possibilities of functionalization to modulate the response. On the other hand, silicene and hybrid SiC nanomaterials being rooted as stable drug payloads favor covalent functionalization through Si functional site.

2. COMPUTATIONAL METHOD

While many adsorption studies of molecules on 2D materials employ methods with periodic boundary conditions, here the cluster model approach is used which focuses on the local nature of the interaction. As discussed previously,[22] there is no *a priori* reason that one approach is more appropriate or better. Depending on the problem at hand, one method might offer advantages over the other. For example, a cluster model would not be useful to study transport properties of metals, but it can provide detailed descriptions of properties and interactions that are localized in nature like adsorption processes[23,24] or core level shifts.[25] When properly handled, the cluster approach has the advantage that the whole toolkit of modern quantum chemistry with many comparisons to experimental data is available to give reasonable estimates about the quality of the results.

The choice of cluster size is an important consideration for the accuracy and reliability of the cluster model. Before the clusters with three neighboring regions around the central hexagon were chosen (i.e., X96H24 clusters with H atoms terminating the edge atoms), some exploratory calculations were performed on smaller X54H18 cluster with only two regions of neighbors around the central hexagon.

As was found before for hydrogen and proton interactions on graphene,[22] the smaller cluster models give virtually the same result for some local properties like average bond length or the PZA−substrate binding energy except for the silicene system (see Table S1, Supporting Information). In order to allow for a consistent comparison between all systems, X96H24 was chosen as common cluster size to study the binding energy trend for the various 2D materials investigated in this paper.

A nonlocal property like the gap size converges slower (see Table S1), but as has been studied before,[26,27] the bulk gaps are approached with increase in cluster size by an increase in the HOMO energy level and a decrease in LUMO of the system.

Calculations were performed using density functional theory (DFT) within the generalized gradient approximation in the Perdew, Burke, and Ernzerhof (PBE) parametrization.[28] Since inclusion of a van der Waals (vdW) dispersion correction is necessary for systems governed by $\pi-\pi$ stacking alignments, semiempirical dispersion corrections to DFT developed by Grimme (D2)[29,30] were used. All calculations were performed with GAUSSIAN09 code.[31] In addition, the polarizable continuum model (PCM)[32] with water solvent represented by a homogeneous continuum medium with a dielectric constant of 78.36 was employed to simulate the biological environment for the PZA conjugated complexes. The optical properties of bioconjugated complexes were calculated using the time-dependent DFT method[33] as implemented in GAUSSIAN09. We considered 100 singlet excited states for PZA and 300 singlet excited states for the bare and conjugated clusters for calculations of the UV−vis spectrum.

To determine the preferred adsorption sites of PZA on the various clusters, an extensive configurational search was performed by calculating total energy for several interacting molecular configurations along the plane both parallel and perpendicular to the clusters. It is worth noting a similar procedure has been successfully employed to obtain the equilibrium configurations of the bioconjugated complexes consisting of BN nanostructures (unpublished results).

The BE (ΔE_b) of PZA on the 2D clusters is calculated as follows:

$$\Delta E_b = E_{\text{PZA/2D cluster}} - (E_{\text{PZA}} + E_{\text{2D cluster}}) \quad (1)$$

where $E_{\text{PZA/2D cluster}}$ is total energy of the complex; E_{PZA} and $E_{\text{2D cluster}}$ are total energy values of PZA and bare 2D cluster, respectively. Negative value of ΔE_b predicts stability of the complex.

3. RESULTS AND DISCUSSION

3.1. Structural Properties. PZA is nearly a planar molecule with the $-CONH_2$ tilted off plane by dihedral angle of 29.86° (Figure 1). It exhibits four polymorphic forms

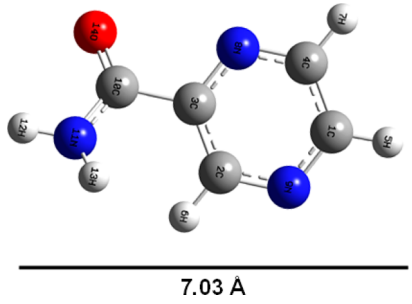

Figure 1. Equilibrium configuration of a PZA molecule in the solvated phase.

ranging from α to δ depending on the reaction conditions and temperature,[34] and its structural stability is rendered from intramolecular hydrogen bonding. In the solvated phase, the calculated structural parameters of PZA are in good agreement with the X-ray crystallographic data[35,36] and prior theoretical study[37] performed at the B3LYP/6-31G(d) level with GAUSSIAN98W (Table S2). The calculated energy gap between highest occupied molecular orbital (HOMO) and

DOI: 10.1021/acs.jpcc.6b06000
J. Phys. Chem. C XXXX, XXX, XXX−XXX

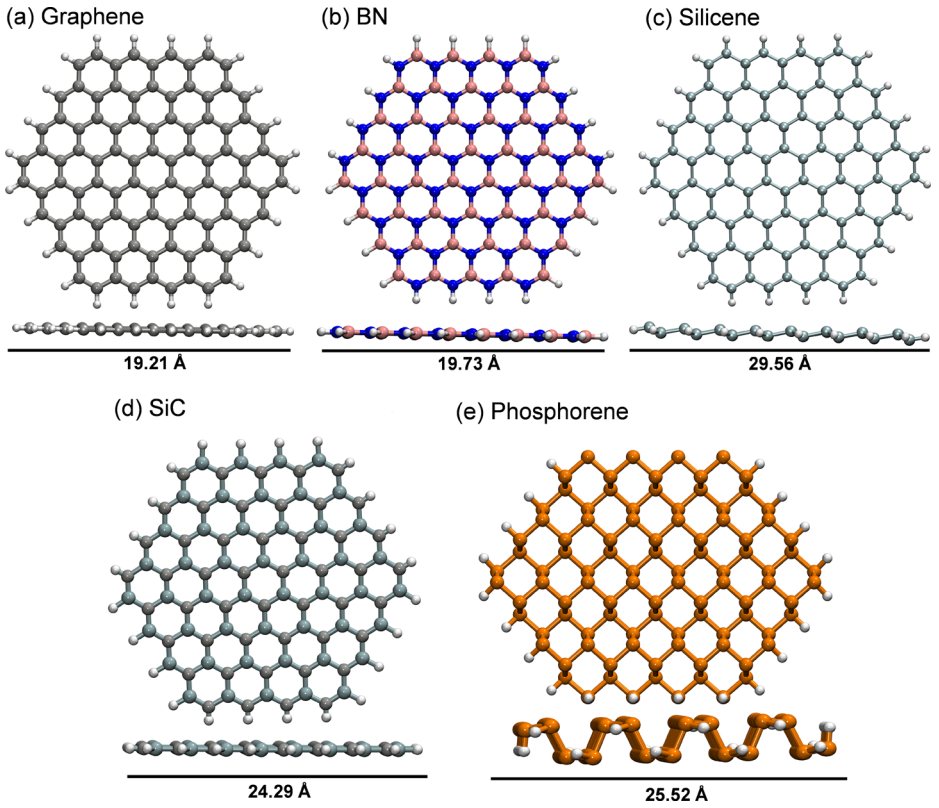

Figure 2. Equilibrium configuration of (a) graphene, (b) BN, (c) silicene, (d) SiC, and (e) phosphorene clusters calculated at the level of DFT(PBE)-D2.

lowest unoccupied molecular orbital (LUMO) is 3 eV, and the dipole moment is 4.47 D, suggesting asymmetric charge distribution in the molecule.

Figure 2 displays the equilibrium configurations of 2D clusters obtained at the level of DFT (PBE)-D2 theory. Both graphene and BN cluster have planar structures with C−C and B−N bond lengths of 1.42 and 1.45 Å, respectively. Silicene has a low puckered geometry with Si−Si bond length of 2.28 Å, buckling distance of 0.51 Å, and the dihedral puckering angle of 39.1°. For the nonplanar configurations, we define the buckling distance to be the distance at which an atom is offset from a completely planar geometry whereas the dihedral puckering angle is defined as the puckering distortion of the six-membered silicene ring induced by buckling. The calculated Si−Si bond length of 2.28 Å is in good agreement with prior periodic DFT study.[38] Earlier reports[39] calculated the buckling distance (height) to be 0.44 Å (without hydrogen) and 0.72 Å (with hydrogen), implying the predominance of sp^3 over sp^2 hybridization in the lattice. Also, the buckling distance in the hexagonal silicene is reported to be 0.53 Å.[40] Likewise, the calculated value of puckering angle is in consistent agreement with previous DFT calculation using the periodic supercell model.[41]

The SiC cluster is a planar configuration with Si−C bond length of 1.80 Å, which is intermediate between the bond lengths of graphene and silicene. Phosphorene prefers a highly puckered structure with a dihedral puckering angle of ∼78°−79°, buckling distance of ∼2.2 Å, and (in-plane) P−P bond length of 2.24 Å in the equilibrium configuration (Table 1).

3.2. Bioconjugated Complexes. To simulate the biological environment, a water solvent was modeled as continuum medium (not discrete water molecules) within the polarizable continuum model (PCM).[32] In order to discuss the effect of solvation, we compare in Table S3 the results for equilibrium distances and binding energies for the gas and solvated phases of the PZA/graphene and PZA/BN complexes. As can be seen, the water solvent has very little effect on the equilibrium distance. A decrease of 0.03 Å from 3.16 Å in the gas phase to 3.13 Å in the solvated phase of PZA/graphene and of 0.07 Å from 3.09 to 3.02 Å for PZA/BN. In both cases, the solvation decreases the binding energies by about 10%. The results for the equilibrium distances were obtained using dispersion correction terms. When compared to the previous gas-phase

Table 1. Calculated Bond Length (Å), Lattice Constant (Å), and Buckling Distance (Å) for the Pristine 2D Clusters

2D clusters	point group symmetry	bond length (Å)	lattice constant (Å)	buckling distance (Å)
graphene				
C−C	D_{6h}	1.42	2.47	
BN				
B−N	C_{3h}	1.45	2.52	
B−H		1.20		
silicene				
Si−Si	C_1	2.28	3.86	0.51
SiC				
Si−C	D_{3h}	1.80	3.11	
phosphorene				
(in-plane) P−P	C_{2h}	2.24		
(out-of-plane) P−P		2.29	3.56	2.2

DOI: 10.1021/acs.jpcc.6b06000
J. Phys. Chem. C XXXX, XXX, XXX−XXX

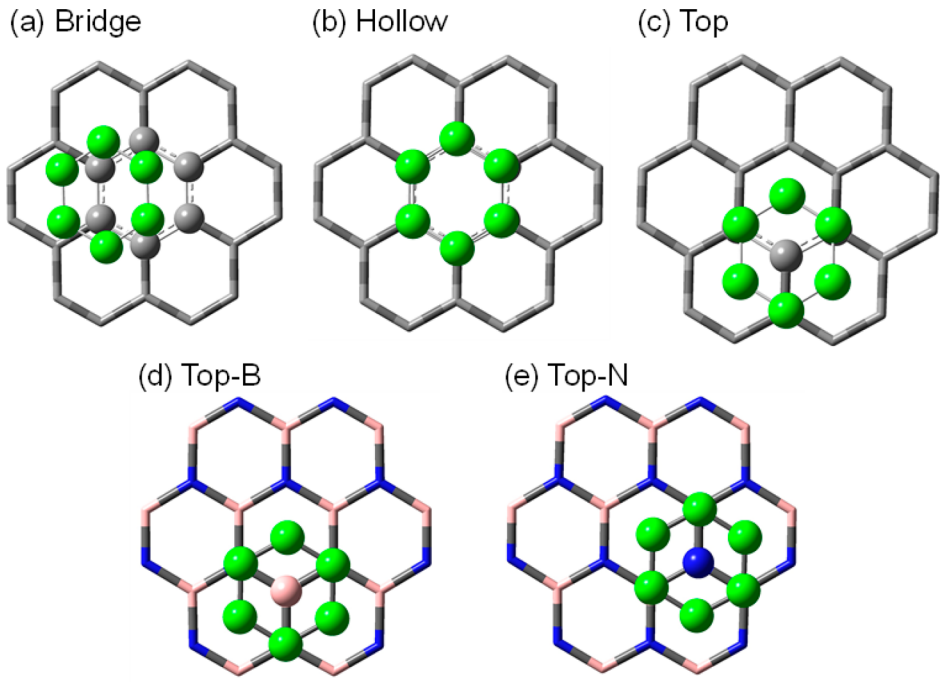

Figure 3. Preferred binding sites for PZA along the surface of 2D cluster: (a) Bridge, (b) Hollow (AA conformation), (c) Top (AB conformation), (d) Top-B, and (e) Top-N sites.

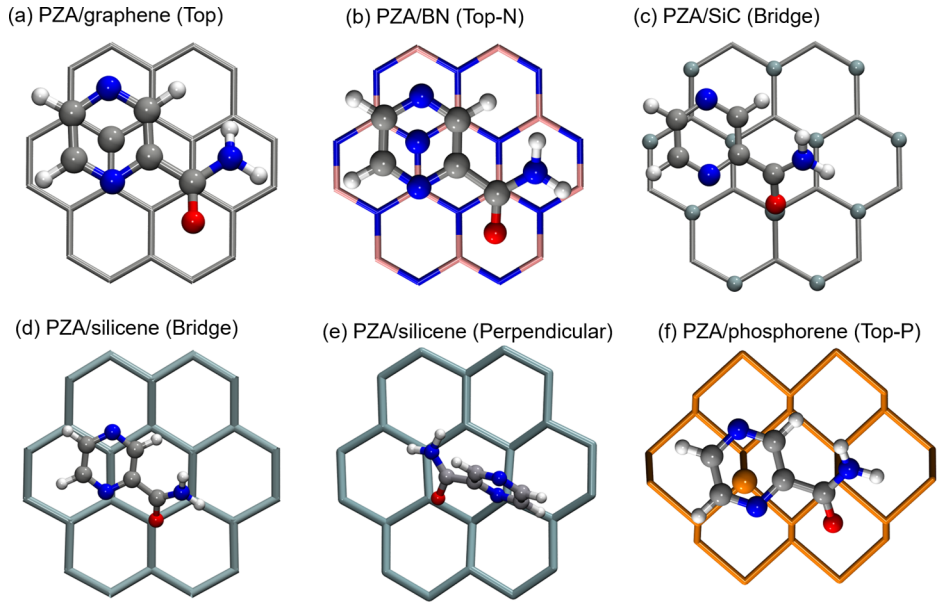

Figure 4. Close views of the equilibrium configurations of PZA-conjugated 2D material complexes: (a) graphene, (b) BN, (c) SiC, (d) silicene (parallel), (e) silicene (perpendicular), and (f) phosphorene clusters.

DFT study (3.81 Å for the graphene and 3.58 Å for BN system),[42] they demonstrate the importance of including dispersion effects for the bioconjugated complexes considered.

The preferred sites of 2D materials interacting with PZA are exclusively taken to be the so-called Bridge, Hollow, and Top sites[43] as shown in green in Figure 3. The probe aromatic ring (i) can be oriented along a bridging bond of the honeycomb lattice sharing two bonded atoms—bridge site (Figure 3a), (ii) is stacked at a AA conformation—hollow site (Figure 3b), and (iii) is stacked at a AB conformation being placed exactly above the surface atom (Figure 3c, Top site). Our choice of the stacking sites is guided by previous reports of organic molecules interacting with graphene and carbon nanotubes.[44−46] Note that the preferred stacking mode for aromatic moieties is likely to be the parallel orientation which allows maximum electron overlap between interacting moieties. Apart from the parallel orientation of the molecule, a perpendicular orientation of PZA on the cluster was also considered in our calculations.

The equilibrium configurations of the bioconjugated complexes are displayed in Figure 4 showing the preferred interaction sites of 2D clusters. For example, PZA prefers the Top site (Figure 4a) of graphene with an average nearest-neighbor distance of 3.13 Å in the solvated phase (Table 2). In the periodic models of armchair (zigzag) carbon nanotubes, the

DOI: 10.1021/acs.jpcc.6b06000
J. Phys. Chem. C XXXX, XXX, XXX−XXX

Table 2. Calculated Structural Parameters of PZA-Conjugated 2D Materials: Nearest-Neighbor Distance (d, Å), Binding Energy (ΔE_b, eV), Charge Transfer from PZA to the Cluster, and Dipole Moment (D, Debye)

preferred binding site (Figure 3)	nearest-neighbor distance (d, Å)	ΔE_b (eV)	charge transfer ($\|e\|$)	dipole moment (D)
graphene (Top) site	3.13	−0.68	0.04	4.00
BN cluster (Top-N) site	3.02	−0.84	0.07	4.94
silicene (Bridge) site	1.87	−1.41	0.46	14.51
SiC (Bridge) site	1.92	−1.10	0.37	11.25
phosphorene (Top-P) site	3.42	−0.66	0.17	5.13

calculated distance between PZA and tubular surface was 2.98 (3.17) Å.[47] It is quite interesting to find that calculations involving the hollow and bridge sites together with perpendicular orientations of PZA converge to the preferred AB stacking (Top site), suggesting dominance of the vdW interactions. The overall planarity of graphene is retained in the complex.

For PZA adsorption onto BN cluster, four major stacking sites were considered: Bridge, Hollow, Top-B, and Top-N as illustrated in Figure 3d,e along with the perpendicular orientation of the molecule interacting with the cluster. The Top-N site of BN cluster (Figure 4b) was preferred for PZA with the nearest-neighbor distance of 3.02 Å (Table 2). The perpendicular orientation of PZA flipped to Top-N site during geometry optimization exemplifying the site specificity of BN cluster toward PZA.

For PZA-conjugated SiC (Figure 4c), the planarity of SiC cluster is nearly retained, though we find noticeable rippling within a localized region with a Si atom protruding out of SiC basal plane by ∼0.42 Å (see Supporting Information, Figure S1a). The Si−O_{PZA} covalent bond restricts the flexibility of the pyrazine ring to the preferred bridge site (binding energy of −1.10 eV) followed by the other competing sites in the range of −1.05 to −1.08 eV.

The localized rippling predicted in SiC cluster is substantially enhanced for silicene (Figure 4d) where the calculated results show significant local distortions in silicene within the proximity of PZA. It appears that the localized buckling within silicene is associated with the formation of Si−O_{PZA} bond which pulls a Si atom out-of-plane by ∼0.73 Å (Figure S1b). The Si−O_{PZA} and Si−N_{PZA} bond distances are 1.87 and 3.64 Å, respectively. Interestingly, we find the perpendicular orientation of PZA (Figure 4e) to be nearly degenerate in energy with the parallel one. In the perpendicular orientation for O_{PZA} approaching the cluster, the Si−O_{PZA} and Si−N_{PZA} bond distances are 1.94 and 2.24 Å, respectively. Kaloni et al.,[48] showed that benzene and toluene molecules interacting with silicene physisorbed at the hollow site at an interacting distance of 3.41 and 3.35 Å with localized distortions within the silicene monolayer. On the other hand, adsorption of benzene onto silicene as reported by Stephan et al.,[5] proceeds through a cycloaddition reaction, and benzene adopts a butterfly configuration mediated through the Si−C covalent bond. In our study, PZA prefers both parallel and perpendicular orientations, which could be due to the constituent O and N atoms of PZA governing the interaction resulting in the formation of strongly bound complexes onto silicene.

Lastly, PZA prefers the Top-P site of phosphorene (Figure 4f) with the nearest-neighbor distance of 3.42 Å and the binding energy of −0.66 eV (Table 2). The perpendicular orientation flips back to the Top-P (AB stacking) configuration as was the case with graphene and BN.

Overall, PZA appears to be physisorbed on 2D materials with the exception of silicene and SiC clusters. The BN cluster, because of its ionic character, yields the binding energy of −0.84 eV, followed by graphene (−0.68 eV) and phosphorene (−0.66 eV) in the PZA-conjugated complexes. The calculated nearest-neighbor distance between PZA and these clusters is beyond 3.0 Å, which falls well within the weakly bonded regime of interaction.

The Mulliken charge analysis shows the charge transfer from PZA to cluster to be minimal in the range of ∼0.04−0.2 $|e|$ for graphene, BN, and phosphorene. For silicene and SiC cluster, the calculated charge transfer is ≈0.5 and ≈0.4 $|e|$, respectively. In fact, the charge transfer and magnitude of the dipole moment bear direct correlation to one another; e.g., the calculated dipole moment of PZA-conjugated silicene is ∼15 D, which is solely dominated by PZA inducing polarizability within the conjugated systems. The other 2D materials also demonstrate increase in polarizability upon functionalization with PZA, suggesting the influence of physisorbed PZA on the 2D clusters.

3.3. Electronic Properties. Figure 5 shows the frontier molecular orbital levels around HOMO and LUMO of bare PZA and its bioconjugated complexes in order to analyze changes in the energy levels of the functionalized complexes. The red dashed arrows correspond to energy gap of bare PZA, and PZA functionalized 2D clusters, and pink arrows correspond to midgap states within the energy gap of PZA/BN and PZA/SiC complexes introduced by the PZA molecule.

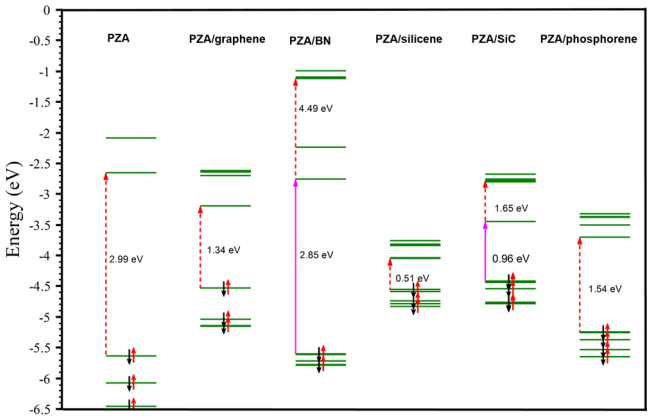

Figure 5. Molecular orbital level diagram of PZA, PZA/graphene PZA/BN, PZA/silicene, PZA/SiC, and PZA/phosphorene complexes. The red dashed arrows correspond to energy gap of bare PZA and PZA functionalized 2D clusters, and pink arrows correspond to midgap states within the energy gap of PZA/BN and PZA/SiC complexes introduced by PZA molecule.

For the bare 120-atom clusters of graphene, BN, silicene, SiC, and phosphorene the HOMO−LUMO gaps are 1.34, 4.49, 0.53, 1.65, and 1.52 eV, respectively (see Table S1). As has been discussed in the Computational Method section, these cluster gaps will approach the bulk gaps with increase in cluster

DOI: 10.1021/acs.jpcc.6b06000
J. Phys. Chem. C XXXX, XXX, XXX−XXX

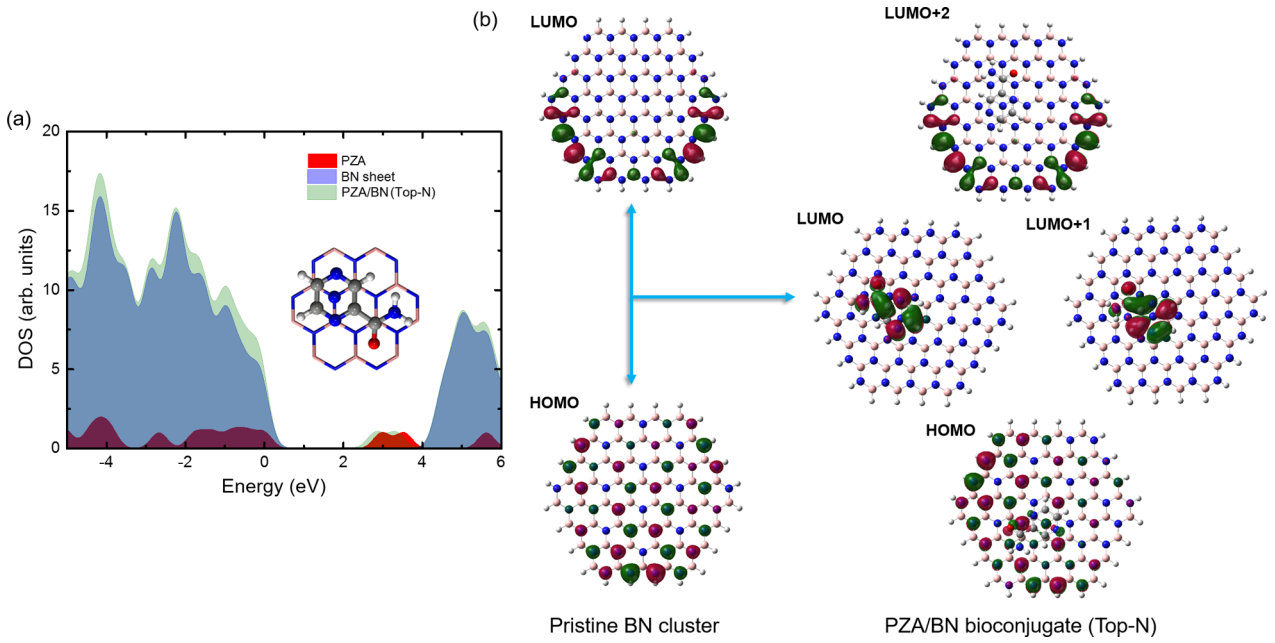

Figure 6. Combined density of states (DOS) of (a) PZA/BN bioconjugates and (b) Frontier orbital analysis corresponding to HOMO and LUMO of pristine BN cluster (left panel) and PZA/BN bioconjugate at Top-N site from HOMO to LUMO+2 states.

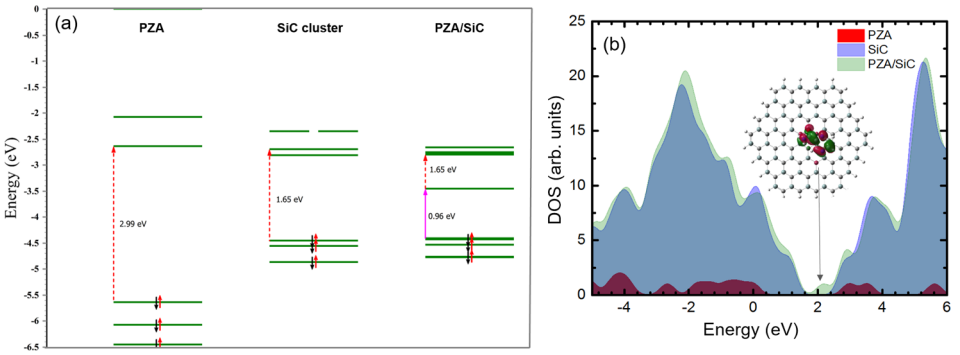

Figure 7. (a) Molecular orbital energy levels of PZA, SiC cluster, and PZA/SiC bioconjugate at the DFT-D2 level. The red arrows depict the electron transition from HOMO to LUMO energy states. (b) Density of states (DOS) of PZA/SiC system corresponding to bridge adsorption site (isovalue = 0.1 eV). The inset shows the LUMO orbital isosurface for the PZA/SiC complex.

size (zero band gaps for graphene and silicene, finite gaps for BN, SiC, and phosphorene). If we define "gaps" for the functionalized complexes as the difference between the HOMO and LUMO level with nanomaterial (C, BN, Si, etc.) character, we find that they remain virtually unchanged upon functionalization with PZA (see Figure 5). However, in the wide gap of the PZA functionalized BN complex, two new states appear which have PZA character. The lower one of these allows for a first excitation at 2.85 eV. In the gap of the PZA/SiC system, due to the PZA−SiC chemisorption interaction, one new state appears with PZA character (with an excitation energy of 0.96 eV). Figures 6 and 7 visualize the appearance and nature of these midgap states in more detail.

Figure 6b displays the frontier orbitals for PZA conjugated BN cluster. A mixing of BN and PZA orbitals forms HOMO. The midgap states, LUMO and LUMO+1, are associated only with PZA, and LUMO+2 is associated with BN cluster and is about 4.5 eV above HOMO.

In a similar way, the frontier orbitals of the other PZA conjugated complexes have been analyzed (see Figures S2−S5). In the PZA functionalized graphene, the frontier orbitals remain associated with graphene, and contributions from PZA show up for LUMO+2. In pristine silicene, the frontier orbitals are localized on the outer ring with the exception of HOMO (Figure S3) which is a bonding orbital localized along the Si−O_{PZA} region. As discussed above, PZA conjugated SiC also exhibits a PZA induced midgap state (Figure 7a).

The midgap state in PZA/SiC can be further interpreted from the DOS and the frontier orbital isosurface corresponding to LUMO (Figure 7b) which represents contribution solely from the adsorbed PZA molecule rather than the SiC cluster. LUMO+1 and LUMO+2 show a combined contribution of PZA and SiC (Figure S4). The PZA introduced midgap state is indicated by the black arrow in Figure 7b.

In phosphorene, HOMO and HOMO−1 are localized around the edges, whereas LUMO is formed by contributions from the inner phosphorene buckled honeycombs (see Figure S5).

3.4. Optical Properties. The optical properties of the bioconjugated complexes are calculated using the time-dependent density functional theory (TDDFT) which has been successfully applied to study the lowest excitations and

DOI: 10.1021/acs.jpcc.6b06000
J. Phys. Chem. C XXXX, XXX, XXX−XXX

absorption spectra of nanomaterials including graphene quantum dots.[49] A total of 100 singlet excited states were considered for PZA, and 300 singlet excited states were examined for the pristine and PZA-conjugated clusters to account for the major excitations in the UV−vis range. A level broadening[50] of about 0.08 eV was used to plot the absorption spectrum as shown in Figure 8.

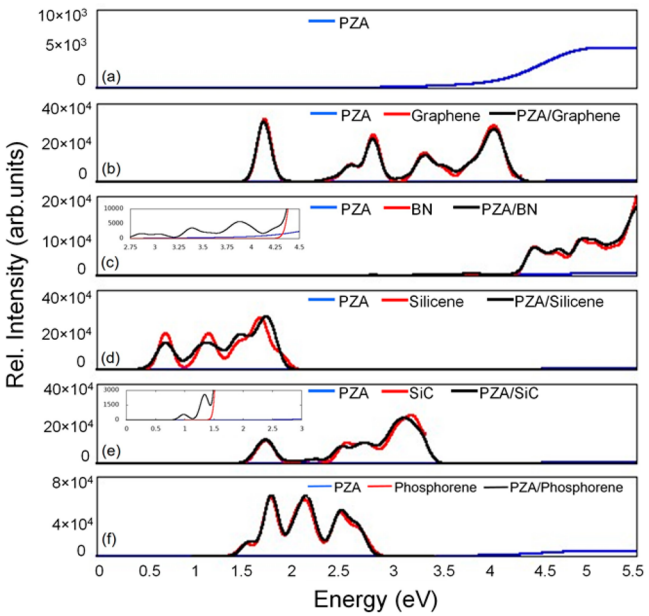

Figure 8. TDDFT calculated absorption spectrum of PZA adsorbed onto the 2D clusters (bottom to top panel: PZA/BP, PZA/SiC, PZA/silicene, PZA/BN, PZA/graphene, and bare PZA). Zoom-in of the absorption spectrum has been depicted for PZA/SiC (0−3.0 eV) and PZA/BN in the region of 2.75−4.5 eV.

The oscillator strength (f)[51,52] which correlates to a particular electronic transition is defined by

$$f = \frac{4m_e c\varepsilon_0}{N_A e^2} B \tag{2}$$

where m_e is the mass of electron, ε_0 the vacuum permittivity, c the speed of light, e the electronic charge, N_A Avogadro's number, and B the molar absorption coefficient. The oscillator strengths vary in the range of 0 → 1, where $f = 1$ corresponds to allowed transitions and $f \sim 0$ to be the forbidden transitions.

In bare PZA (Figure 8a), the first singlet excited states with weak oscillator strengths ($f = 0.001$) are observed at 3.1 and 3.5 eV, followed by six "dark" singlets with $f = 0$. The first prominent absorption peak for PZA at 5.8 eV with $f = 0.12$ corresponds to transition from HOMO−3 → LUMO+1.

For graphene cluster (red line in Figure 8b), we find two dark singlets around 1.35−1.48 eV below the first two degenerate "bright" excitons at 1.74 eV (with $f = 1.1$) showing a good agreement with the structures calculated for graphene quantum dots.[49] The first doubly degenerate "bright" singlet at 1.74 eV corresponds to two degenerate transitions (HOMO−1 → LUMO and HOMO−1 → LUMO+1) followed by multiple "dark" singlet excitons before the onset of a doubly degenerate absorption shoulder at 2.87 eV (with $f = 0.81$). The main contribution of PZA in the optical absorption of graphene is that it breaks the symmetry of pristine graphene and lifts the degeneracy of the excitations. In the PZA/graphene complex, the first doubly degenerate "bright" exciton remains unperturbed at 1.73 eV (with $f \approx 1.01$), which corresponds to transition from HOMO−1 → LUMO+1 and LUMO states, followed by singlet shoulder at 2.87 eV (with $f = 0.73$). The dark states which corresponded to symmetry-forbidden transitions in the pristine graphene acquire finite oscillator strength upon physisorption of PZA, which is reflected in the absorption spectrum of the PZA/graphene complex with slightly lowered intensity and peak broadening.

A similar effect of symmetry breaking due to chemisorbed PZA on the optical absorption spectra of silicene is predicted. The doubly degenerate peak at 0.71 eV (with $f = 0.57$) for the pristine silicene (Figure 8d), which corresponds to electronic transitions from HOMO−1 → LUMO+1 and LUMO states, splits into two shoulder peaks at 0.67 eV (with $f = 0.24$) for transition from HOMO−1 → LUMO+1 and 0.69 eV (with $f = 0.40$) for HOMO−1 → LUMO transitions, followed by the broad peak at 1.15 eV (with $f = 0.25$). The quenching in the absorption spectra with significant broadening and subsequent lowering in the peak intensity for silicene is accounted from the chemisorbed PZA molecule on the surface.

We expect modifications in the absorption spectrum for PZA/BN and PZA/SiC complexes due to appearance of midgap states within the band gap (Figure 5). In the PZA/BN system (Figure 8c), the onset of first allowed singlet excitation is at 2.85 eV (see inset in Figure 8) with low shoulders peaks between 3.0 and 3.3 eV (with $f < 0.01$), well within the energy gap of the pristine BN cluster. The next doubly degenerate peak is obtained at 4.52 and 4.54 eV (with $f = 0.16$ and 0.13), which corresponds to transitions from HOMO → LUMO+2 followed by singlet states having weak oscillator strengths. Similarly, for the PZA/SiC system (Figure 8e), first excitations are found at 0.96 eV (with $f = 0.001$) and 1.35 eV ($f = 0.01$) which are contributed from the chemisorbed PZA molecule before they merge with the pristine SiC spectrum at 1.71 eV (with $f = 0.18$) (see inset in Figure 8). Therefore, PZA functionalization leads to broadening of absorption peak of pristine SiC cluster. For the PZA/phosphorene complex, the onset of the absorption peak is at 1.58 eV (with $f = 0.07$) followed by intense peak at 1.81 eV ($f = 0.34$) which remains unperturbed after physisorption of PZA on the cluster (Figure 8f).

The influence of the weakly adsorbed PZA on the UV−vis spectrum of the bioconjugated complexes is quite subtle and may not be easily detectable. In the case of PZA interacting with silicene the Si 2p core-level photoemission spectroscopy might serve a better tool to analyze the extent of distortion in the functionalized complex. Note that core-level shifts have been used to analyze changes in the environment of atoms due to adsorption, surfaces, or any other differences in neighboring Si atoms. In the simple "initial state" approximation, the Si 2p core-level shift is simply calculated as difference between the 2p core-level energies of Si atoms in different environments, assuming that effects of final states can be neglected or canceled.

The pristine silicene $Si_{96}H_{24}$ cluster has 288 p states between −94.88 eV (inner Si atoms) and −94.68 eV (Si atoms at the edges). The absorption of PZA leads to a significant core-level shift of −0.74 eV toward −95.62 eV for the 2p orbital of the Si atom bonding to the oxygen atom of PZA and to a shift of +0.35 eV toward a higher binding energy of −94.53 eV for neighboring Si atoms which should be easily detectable experimentally. In general, care must be taken in explaining

DOI: 10.1021/acs.jpcc.6b06000
J. Phys. Chem. C XXXX, XXX, XXX−XXX

the direction of core level shifts,[25,53,54] but in the PZA adsorption case a simple electrostatic picture seems to explain it: the binding of PZA leads to a charge transfer of overall ∼0.5 *e* from PZA to silicene and significant local geometry deformation in the 2d lattice. The local Si atom directly bonding with O of PZA becomes slightly positively charged; the net negative charge of 0.5 *e* gets distributed among the other Si atoms. The slightly positive Si atom has a smaller valence electron population. Its 2p core electrons experience less Coulomb repulsion, and their energy is shifted to lower total binding energy. On the other hand, the 2p electrons of Si atoms that pick up charge experience more electron−electron repulsion and hence shift towards a higher total binding energy.

4. SUMMARY AND CONCLUSION

The aim of this study was to provide an extensive understanding about the nature of interaction in the PZA-functionalized 2D clusters to explore their potential as drug delivery payloads. On the basis of a finite cluster model and density functional theory incorporating the van der Waals dispersion corrections and solvent effects, we demonstrated that PZA selectively binds to the 2D clusters; the extent of adsorption solely governed by site specificity and intrinsic electronic properties of the 2D clusters. PZA is physisorbed on graphene, BN, and phosphorene, with BN having the most favored binding energy value. It is chemisorbed on silicene and SiC with a strong localized puckering along the absorption site mediated by Si−O_{PZA} covalent bond. The BN and SiC clusters are found to be the sole candidates with significant changes in density of states (DOS) around the Fermi level where PZA introduces midgap states. Each of the 2D materials showed a preferred binding site for PZA which correlated with the extent of interaction, charge transfer, and overall polarizability of the bioconjugated complexes in water solvent media. The HOMO−LUMO gaps for graphene, silicene, and phosphorene remain virtually unchanged upon adsorption, whereas they are significantly decreased in BN and SiC clusters due to the appearance of midgap states. The XPS core level shift spectroscopy might serve as a better tool to analyze the chemisorption of PZA onto silicene with a predicted maximum shift of 0.74 eV in Si 2p core levels.

Of the 2D clusters considered, silicene and SiC have been proposed as the stable payloads for PZA favoring covalent functionalization, which in turn would proffer with prolonged drug loading and retention time. *In vitro*, the rupture of covalently bound complexes is feasible with atomic force microscopy (AFM) for mechanochemical cleavage of organic bonds and stress driven-reaction dynamics as reported for graphene.[55] *In vivo*, a reaction similar to the cleavage of functionalized nanotubes[56] (replacing the nanotubes with 2D sensors like SiC and silicene) could remove drug molecules like PZA from the support at the target site. However, from a wider perspective, the weakly bound bioconjugates of PZA with graphene, BN, and phosphorene will have additional possibilities of tailoring the electronic properties for better drug translocation without drastically perturbing the structural morphology of the 2D clusters, thereby opening up divergent possibilities in the nano-bio world of health-related research at the nanoscale.

■ ASSOCIATED CONTENT

Supporting Information

The Supporting Information is available free of charge on the ACS Publications website at DOI: 10.1021/acs.jpcc.6b06000.

Comparison of calculated energy gap, average bond length, and binding energy for selected PZA-conjugated clusters of 72 and 120 atoms in aqueous media (Table S1); calculated structural properties of a PZA molecule in the solvated phase (Table S2); nearest-neighbor distance and binding energies for the gas and solvated (PCM) phases of the PZA/graphene and PZA/BN 120 atom clusters (Table S3); side views of PZA adsorbed onto silicene and SiC clusters (Figure S1); frontier orbital isosurface corresponding to HOMO−1, HOMO, LUMO, LUMO+1, and LUMO+2 for PZA/graphene (Figure S2), PZA/silicene (Figure S3), PZA/SiC (Figure S4), and PZA/phosphorene (Figure S5) bioconjugates (PDF)

■ AUTHOR INFORMATION

Corresponding Authors

*E-mail nabanita16@gmail.com; Tel +1-906-231-5540 (N.S.).
*E-mail pandey@mtu.edu; Tel +1-906-487-2086 (R.P.).

Notes

The authors declare no competing financial interest.

■ ACKNOWLEDGMENTS

The authors thank K. Waters and S. Gowtham for valuable discussions. N.S. kindly acknowledges financial support from Michigan Technological University, Houghton, MI. Computational resources at Michigan Technological University with SUPERIOR high performance computing cluster were used in obtaining the results presented in this study.

■ REFERENCES

(1) Geim, A. K.; Novoselov, K. S. The rise of graphene. *Nat. Mater.* **2007**, *6*, 183−191.
(2) Bonaccorso, F.; Sun, Z.; Hasan, T.; Ferrari, A. C. Graphene photonics and optoelectronics. *Nat. Photonics* **2010**, *4*, 611−622.
(3) Pan, L.; Liu, H. J.; Wen, Y. W.; Tan, X. J.; Lv, H. Y.; Shi, J.; Tang, X. F. First-principles study of cluster and bilayer honeycomb structures of group-IV elements and their binary compounds. *Phys. Lett. A* **2011**, *375*, 614−619.
(4) Cavallo, F.; Delgado, R. R.; Kelly, M. M.; Pérez, J. R. S.; Schroeder, D. P.; Xing, H. G.; Eriksson, M. A.; Lagally, M. G. Exceptional Charge Transport Properties of Graphene on Germanium. *ACS Nano* **2014**, *8*, 10237−10245.
(5) Stephan, R.; Hanf, M. C.; Sonnet, P. Molecular functionalization of silicene/Ag(111) by covalent bonds: a DFT study. *Phys. Chem. Chem. Phys.* **2015**, *17*, 14495−14501.
(6) Cahangirov, S.; Topsakal, M.; Akturk, E.; Sahin, H.; Ciraci, S. Two- and One-Dimensional Honeycomb Structures of Silicon and Germanium. *Phys. Rev. Lett.* **2009**, *102*, 236804.
(7) Shao, Z.-G.; Ye, X.-S.; Yang, L.; Wang, C.-L. First-principles calculation of intrinsic carrier mobility of silicene. *J. Appl. Phys.* **2013**, *114*, 093712.
(8) Guzmán-Verri, G. G.; Voon, L. C. L. Y. Electronic structure of silicon-based nanostructures. *Phys. Rev. B: Condens. Matter Mater. Phys.* **2007**, *76*, 075131.
(9) Drummond, N. D.; Zólyomi, V.; Fal'ko, V. I. Electrically tunable band gap in silicene. *Phys. Rev. B: Condens. Matter Mater. Phys.* **2012**, *85*, 075423.

DOI: 10.1021/acs.jpcc.6b06000
J. Phys. Chem. C XXXX, XXX, XXX−XXX

(10) Liu, C. C.; Feng, W.; Yao, Y. Quantum spin Hall effect in silicene and two-dimensional germanium. *Phys. Rev. Lett.* **2011**, *107*, 076802.
(11) Peng, Q.; Wen, X.; De, S. Mechanical stabilities of silicene. *RSC Adv.* **2013**, *3*, 13772−13781.
(12) Xia, F.; Wang, H.; Jia, Y. Rediscovering Black Phosphorus as an Anisotropic Layered Material for Optoelectronics and Electronics. *Nat. Commun.* **2014**, *5*, 4458.
(13) Li, L.; Yu, Y.; Ye, G. J.; Ge, Q.; Ou, X.; Wu, H.; Feng, D.; Chen, X. H.; Zhang, Y. Black Phosphorus Field-Effect Transistors. *Nat. Nanotechnol.* **2014**, *9*, 372−377.
(14) Wang, G.; Slough, W. J.; Pandey, R.; Karna, S. P. Degradation of phosphorene in air: understanding at atomic level. *2D Mater.* **2016**, *3*, 025011.
(15) Wirtz, L.; Marini, A.; Rubio, A. Optical Absorption of hexagonal Boron Nitride and BN nanotubes. *AIP Conf. Proc.* **2005**, *786*, 391−395.
(16) Bianco, A.; Kostarelos, K.; Prato, M. Applications of carbon nanotubes in drug delivery. *Curr. Opin. Chem. Biol.* **2005**, *9*, 674−679.
(17) Kurapati, R.; Kostarelos, K.; Prato, M.; Bianco, A. Biomedical Uses for 2D Materials Beyond Graphene: Current Advances and Challenges Ahead. *Adv. Mater.* **2016**, *28*, 6052.
(18) Cole, S. T., Eisenach, K. D., McMurray, D. N., Jacobs, W. R., Jr., Eds.; *Tuberculosis and the Tubercle Bacillus*; ASM Press: Washington, DC, 2005.
(19) American Thoracic Society/Centers for disease control and prevention/Infectious diseases society of America: treatment of tuberculosis. *Am. J. Respir. Crit. Care Med.* **2003**, *167*, 603−662.
(20) Petrella, S.; Gelus-Zietal, N.; Maudry, A.; Laurans, C.; Boudjelloul, R.; Sougakoff, W. Crystal Structure of the Pyrazinamidase of Mycobacterium tuberculosis: Insights into Natural and Acquired Resistance to Pyrazinamide. *PLoS One* **2011**, *6*, e15785.
(21) Wheate, N. J.; Vora, V.; Anthony, N. G.; McInnes, F. J. Host−guest complexes of the antituberculosis drugs pyrazinamide and isoniazid with cucurbit[7]uril. *J. Inclusion Phenom. Mol. Recognit. Chem.* **2010**, *68*, 359−367.
(22) Seel, M.; Pandey, R. Proton and hydrogen transport through two-dimensional clusters. *2D Mater.* **2016**, *3*, 025004.
(23) Seel, M.; Bagus, P. S. Adsorption and surface penetration of atomic hydrogen at the open site of Si(111): An ab initio cluster-model study. *Phys. Rev. B: Condens. Matter Mater. Phys.* **1981**, *23*, 5464.
(24) Seel, M.; Bagus, P. S. Ab initio cluster study of the interaction of fluorine and chlorine with the Si(111) surface. *Phys. Rev. B: Condens. Matter Mater. Phys.* **1983**, *28*, 2023.
(25) Bagus, P. S.; Seel, M. Molecular-orbital cluster-model study of the core-level spectrum of CO adsorbed on copper. *Phys. Rev. B: Condens. Matter Mater. Phys.* **1981**, *23*, 2065.
(26) Peng, X.-H.; Nayak, S. K.; Alizadeh, A.; Varanasi, K. K.; Bhate, N.; Rowland, L. B.; Kumar, S. K. First-principles study of the effects of polytype and size on energy gaps in SiC nanoclusters. *J. Appl. Phys.* **2007**, *102*, 024304.
(27) Corain, B.; Schmid, G.; Toshima, N. *Metal Nanoclusters in Catalysis and Materials Science: The Issue of Size Control*, 1st ed.; Elsevier: Oxford, 2008.
(28) Perdew, J. P.; Burke, K.; Wang, Y. Generalized gradient approximation for the exchange-correlation hole of a many-electron system. *Phys. Rev. B: Condens. Matter Mater. Phys.* **1996**, *54*, 16533.
(29) Grimme, S. Semiempirical GGA-type density functional constructed with a long-range dispersion correction. *J. Comput. Chem.* **2006**, *27*, 1787−1799.
(30) Grimme, S.; Antony, J.; Ehrlich, S.; Krieg, H. A consistent and accurate *ab initio* parametrization of density functional dispersion correction (DFT-D) for the 94 elements H-Pu. *J. Chem. Phys.* **2010**, *132*, 154104.
(31) Frisch, M. J.; Trucks, G. W.; Schlegel, H. B.; Scuseria, G. E.; Robb, M. A.; Cheeseman, J. R.; Scalmani, G.; Barone, V.; Mennucci, B.; Petersson, G. A.; et al. *Gaussian 09*; Gaussian, Inc.: Wallingford, CT, 2009.
(32) Tomasi, J.; Mennucci, B.; Cammi, R. Quantum mechanical continuum solvation models. *Chem. Rev.* **2005**, *105*, 2999−3094.
(33) Fabian, J. TDDFT-calculations of Vis/NIR absorbing compounds. *Dyes Pigm.* **2010**, *84*, 36−53.
(34) Tamura, C.; Kuwano, H. Crystallographic data of carboxylic acids and carboxyamides of picoline and pyrazine derivatives. *Acta Crystallogr.* **1961**, *14*, 693.
(35) Takaki, Y.; Sasada, Y.; Watanabe, T. The Crystal Structure of a-Pyrazinamide. *Acta Crystallogr.* **1960**, *13*, 693−702.
(36) Jarzembska, K. N.; Hoser, A. A.; Kaminski, R.; Madsen, A. Ø.; Durka, K.; Wozniak, K. Combined Experimental and Computational Studies of Pyrazinamide and Nicotinamide in the Context of Crystal Engineering and Thermodynamics. *Cryst. Growth Des.* **2014**, *14*, 3453−3465.
(37) Chiş, V.; Pîrnâu, A.; Jurcâ, T.; Vasilescu, M.; Simon, S.; Cozar, O.; David, L. Experimental and DFT study of pyrazinamide. *Chem. Phys.* **2005**, *316*, 153−163.
(38) Ni, Z.; Zhong, H.; Jiang, X.; Quhe, R.; Luo, G.; Wang, Y.; Ye, M.; Yang, J.; Shi, J.; Lu, J. Tunable band gap and doping type in silicene by surface adsorption: towards tunneling transistors. *Nanoscale* **2014**, *6*, 7609−7618.
(39) Voon, L. C. L. Y.; Sandberg, E.; Aga, R. S.; Farajian, A. A. Hydrogen compounds of group-IV nanosheets. *Appl. Phys. Lett.* **2010**, *97*, 163114.
(40) Ding, Y.; Ni, J. Electronic structures of silicon nanoribbons. *Appl. Phys. Lett.* **2009**, *95*, 083115.
(41) Jose, D.; Datta, A. Structures and Chemical Properties of Silicene: Unlike Graphene. *Acc. Chem. Res.* **2014**, *47*, 593−602.
(42) Saikia, N.; Deka, R. C. Density functional study on noncovalent functionalization of pyrazinamide chemotherapeutic with graphene and its prototypes. *New J. Chem.* **2014**, *38*, 1116−1128.
(43) Zhou, P.-P.; Zhang, R.-Q. Physisorption of benzene derivatives on graphene: critical roles of steric and stereoelectronic effects of the substituent. *Phys. Chem. Chem. Phys.* **2015**, *17*, 12185−12193.
(44) Ershova, O. V.; Lillestolen, T. C.; Bichoutskaia, E. Study of polycyclic aromatic hydrocarbons adsorbed on graphene using density functional theory with empirical dispersion correction. *Phys. Chem. Chem. Phys.* **2010**, *12*, 6483−6491.
(45) Pykal, M.; Jurečka, P.; Karlický, F.; Otyepka, M. Modelling of graphene functionalization. *Phys. Chem. Chem. Phys.* **2016**, *18*, 6351−6372.
(46) Woods, L. M.; Bădescu, Ş. C.; Reinecke, T. L. Adsorption of simple benzene derivatives on carbon nanotubes. *Phys. Rev. B: Condens. Matter Mater. Phys.* **2007**, *75*, 155415.
(47) Saikia, N.; Jha, A. N.; Deka, R. C. Interaction of pyrazinamide drug functionalized carbon and boron nitride nanotubes with pncA protein: a molecular dynamics and density functional approach. *RSC Adv.* **2013**, *3*, 15102−15107.
(48) Kaloni, T. P.; Schreckenbach, G.; Freund, M. S. Large Enhancement and Tunable Band Gap in Silicene by Small Organic Molecule Adsorption. *J. Phys. Chem. C* **2014**, *118*, 23361−23367.
(49) Schumacher, S. Photophysics of graphene quantum dots: Insights from electronic structure calculations. *Phys. Rev. B: Condens. Matter Mater. Phys.* **2011**, *83*, 081417.
(50) Anak, B.; Bencharif, M.; Rabilloud, F. Time-dependent density functional study of UV-visible absorption spectra of small noble metal clusters (Cu_n, Ag_n, Au_n, n = 2−9, 20). *RSC Adv.* **2014**, *4*, 13001−13011.
(51) Robinson, J. W. *Atomic Spectroscopy*, 2nd ed.; CRC Press: 1996.
(52) http://alpha.chem.umb.edu/chemistry/ch612/documents/Week4.pdf.
(53) Seel, M. Core-level shifts and their relation to surface effects and dimensionality of a system. *Int. J. Quantum Chem.* **1997**, *63*, 623−629.
(54) Nilsson, V.; Van den Bossche, M.; Hellman, A.; Grönbeck, H. Trends in adsorbate induced core level shifts. *Surf. Sci.* **2015**, *640*, 59−64.
(55) Felts, J. R.; Oyer, A. J.; Hernández, S. C.; Whitener, K. E., Jr.; Robinson, J. T.; Walton, S. G.; Sheehan, P. E. Direct mechanochemical

DOI: 10.1021/acs.jpcc.6b06000
J. Phys. Chem. C XXXX, XXX, XXX−XXX

cleavage of functional groups from graphene. *Nat. Commun.* **2015**, *6*, 6467.
(56) Sun, Y.-P.; Fu, K.; Lin, Y.; Huang, W. Functionalized Carbon Nanotubes: Properties and Applications. *Acc. Chem. Res.* **2002**, *35*, 1096−1104.

DOI: 10.1021/acs.jpcc.6b06000
J. Phys. Chem. C XXXX, XXX, XXX−XXX